

Nanocrystalline $\text{BaCo}_3(\text{VO}_4)_2(\text{OH})_2$ with a Kagome lattice of Co(II) ions: synthesis, crystal structure and magnetic properties

R. Dessapt,^{*,a} L. Lajaunie,^{b,c} J. J. Calvino,^{b,c} P. Deniard,^a I. Trenque^a and C. Payen^{*,a}

^aUniversité de Nantes, CNRS, Institut des Matériaux Jean Rouxel, IMN, F-44000 Nantes, France

^bDepartamento de Ciencia de los Materiales e Ingeniería Metalúrgica y Química Inorgánica, Facultad de Ciencias, Universidad de Cádiz, Campus Río San Pedro S/N, Puerto Real, 11510, Cádiz, Spain.

^cInstituto Universitario de Investigación de Microscopía Electrónica y Materiales (IMEYMAT), Facultad de Ciencias, Universidad de Cádiz, Campus Río San Pedro S/N, Puerto Real 11510, Cádiz, Spain.

Electronic Supplementary Information

Experimental section

Nitrogen volumetric measurement treated by the Brunauer-Emmett-Teller (BET) approaches were recorded on a micrometrics ASAP 2010 device.

X-ray diffraction (XRD) measurements were performed on a D8 Bruker diffractometer employing the CuK-L3 radiation (Ge (111) monochromator) and a Lynxeye 1D detector in the 5–110° 2θ interval, with 0.014° steps of 3s each. A total acquisition time of about 6 hours was actually necessary to obtain a pattern with a good enough signal to noise ratio because of the fluorescence due to the cobalt-containing sample. The structure refinements was carried out with the Jana2020 software¹, using the Rietveld procedure with the fundamental parameter approach^{2–4} in the $R\bar{3}m$ space group against the structural model of Djordevic et al.⁵ as reported in the ICSD database with the reference number 236321. This method makes possible the deconvolution of the X-ray line profile diffractometer (X-ray energy dispersion and optics) and the specimen itself. Namely, the

CuK-L3 emission profile was calculated from the physics data collected by Cheary et al. and the monochromator setting. The only refined function concerned the specimen itself (crystallite size (Å) and microstrains (%)). The refinement procedure was composed of the calculation of the background (Legendre polynomials), followed by the computation of the sample displacement, cell parameters, crystallite size, and microstrains. The absorption resulting from roughness was then evaluated prior to the Rietveld refinement of the atom positions. Atomic displacement parameters were refined anisotropically for all the atoms excepted oxygens which were constrained to be identical because of their low diffusion factor as compared with those of Ba, Co and V. The Rietveld final figures of merit were a Goodness of fit of 1.09 and a R_{wp} factor of 2.19. Main results are gathered in Table S1.

Table S1. Structural parameters and crystallite size of $\text{BaCo}_3(\text{VO}_4)_2(\text{OH})_2$ NPs.

SG $R\bar{3}m$: $a=5.9085(4)$ Å, $c=21.099(2)$ Å, Cryst. size= $22.2(3)$ nm \perp [001], $18.7(4)$ nm // [001]						
Atom	x	y	z	SOF		U_{iso} Equiv (Å ²)
Ba ₁	0.6667	0.3333	0.8333	1		0.0397 (16)
Co ₁	0.8333	0.6667	0.6667	1		0.038 (2)
V ₁	0.3333	0.6667	0.7537(2)	1		0.012 (2)
O ₁	0.3333	0.6667	0.8327(7)	1		0.0090 (19)
O ₂	0.4989	0.5011	0.7304(3)	1		0.0090
O ₃	0	0	0.71055(5)	1		0.0090
H ₁	0	0	0.7541*	1		0.018*

Aniso. ADP (Å ²)	U^{11}	U^{22}	U^{33}	U^{12}	U^{13}	U^{23}
Ba ₁	0.0460(18)	0.0460(18)	0.027(3)	0.0230(9)	0	0
Co ₁	0.040(2)	0.068(2)	0.017(4)	0.0338(12)	0.0096(12)	0.019(2)
V ₁	0.010(2)	0.010(2)	0.016(4)	0.0049(11)	0	0

*not refined

FT-IR spectra were recorded in the 4000-400 cm^{-1} range on a BRUKER Vertex equipped with a computer control using the OPUS software. FT-Raman spectra were collected at room temperature under an excitation wavelength of 1064 nm (Nd:YAG laser) using a FT-Raman Bruker RFS 100 spectrophotometer. The nominal power was 300 mW. Solid-state FT-Raman spectra were recorded at 4 cm^{-1} resolution over the wavenumber range 50-4000 cm^{-1} , with 400 scan accumulation.

SEM images were performed with a field-emission gun scanning electron microscope JEOL JSM7600F operating at 7 kV.

Aberration-corrected high-resolution scanning transmission electron microscope imaging (HR-STEM) in high-angle annular dark-field (HAADF) mode was performed using a FEI Titan Cubed Themis microscope which was operated at 200 kV. The Themis is equipped with a double Cs aberration corrector, a monochromator, an X-FEG gun, a super EDS detector, and an Ultra High Resolution Energy Filter (Gatan Quantum ERS) which allows for working in Dual-EELS mode. Automatic indexing of the Fast Fourier Transform (FFT) patterns was performed by using the JEMS software.⁶ The probe convergence semiangle was equal to 21 mrad and the inner and outer angles for HAADF imaging were 50 and 200 mrad, respectively. HAADF image simulations were performed with the multislice Dr. Probe software,⁷ and using the XRD-refined structural data as input. Calculations were done in the frozen-lattice approximation. For each slice, 5 frozen lattice states, created by introducing random atomic displacements, were computed to take into account thermal diffuse scattering.

A commercial SQUID magnetometer (Quantum Design, MPMS) was used to collect dc magnetization data. The susceptibility has been defined as the ratio of the magnetization M to the applied field H , $\chi = M/H$. After every isothermal magnetization scan, the sample was heated up to 300 K and then zero-field cooled to the next selected temperature. Isothermal magnetization $M(H)$ curves were linear at low fields, up to $H \approx 300$ Oe at the base temperature (2 K). Thus the temperature-dependent linear susceptibility could be defined as the ratio of the magnetization measured at 100 Oe to the applied field, $\chi = M/H$.

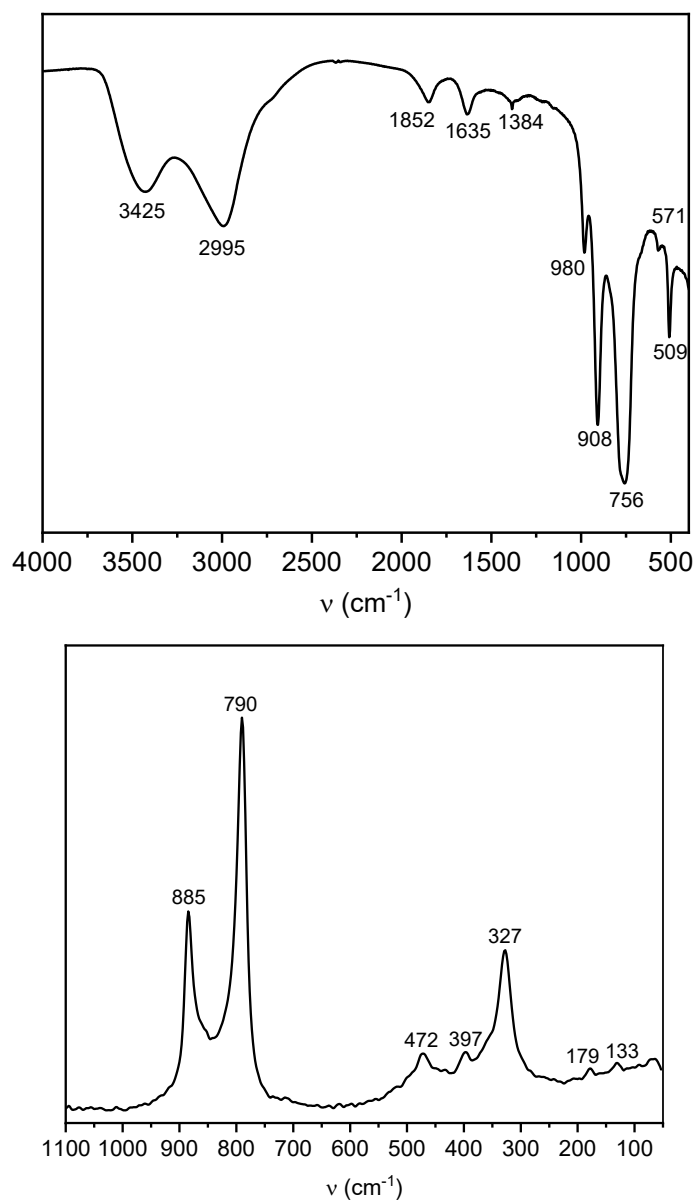


Figure S1. (a) FT-IR (top) and (b) FT-Raman spectra (bottom) of the BaCo₃(VO₄)₂(OH)₂ nanoparticles (NPs).

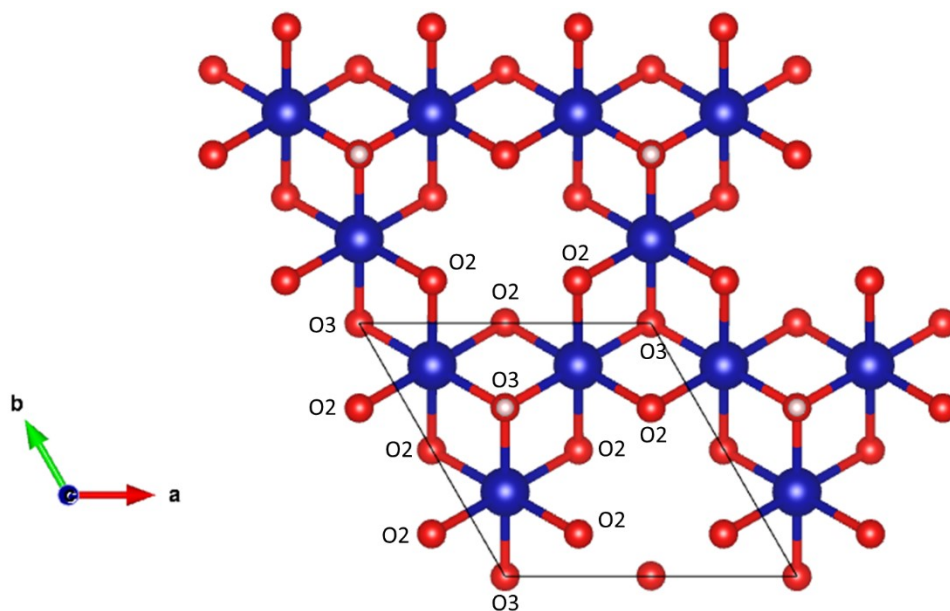


Figure S2. Fragment of a kagome layer in the $\text{BaCo}_3(\text{VO}_4)_2(\text{OH})_2$ crystal structure. Blue, red, and white spheres represent Co, O, and H atoms. Barium and vanadium atoms have been removed for clarity. There are two possible nearest neighbour superexchange interactions with a Co-Co distance of $\approx 2.95 \text{ \AA}$; a Co-O2-Co pathway along the edge of a Co_3 triangle (angle of $85,5(2)^\circ$, $d_{\text{Co-O2}} = 2.176(4) \text{ \AA}$) and a Co-O3-Co pathway in the Co_3 triangle's interior (angle of $99,13(4)^\circ$, $d_{\text{Co-O3}} = 1.9407(6) \text{ \AA}$). Atoms O2 are further bonded to V atoms. Further neighbours intralayers couplings may involve Co-O2-O2-Co pathways.

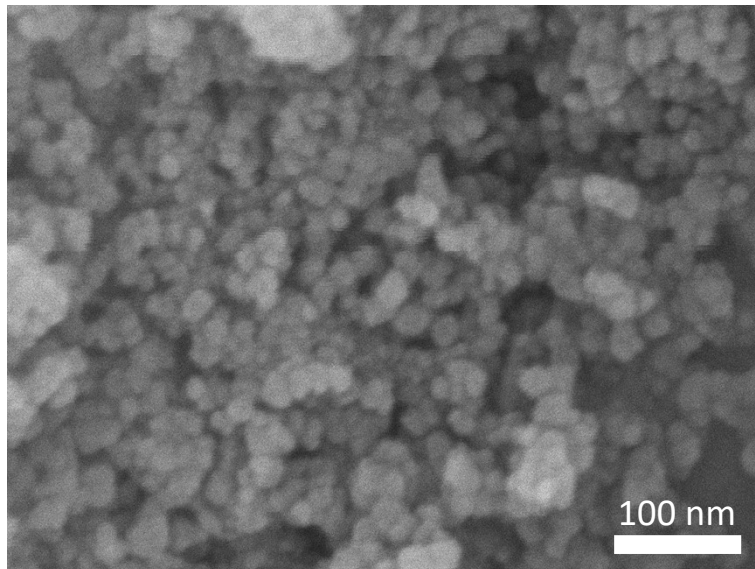


Figure S3. SEM image of the $\text{BaCo}_3(\text{VO}_4)_2(\text{OH})_2$ NPs.

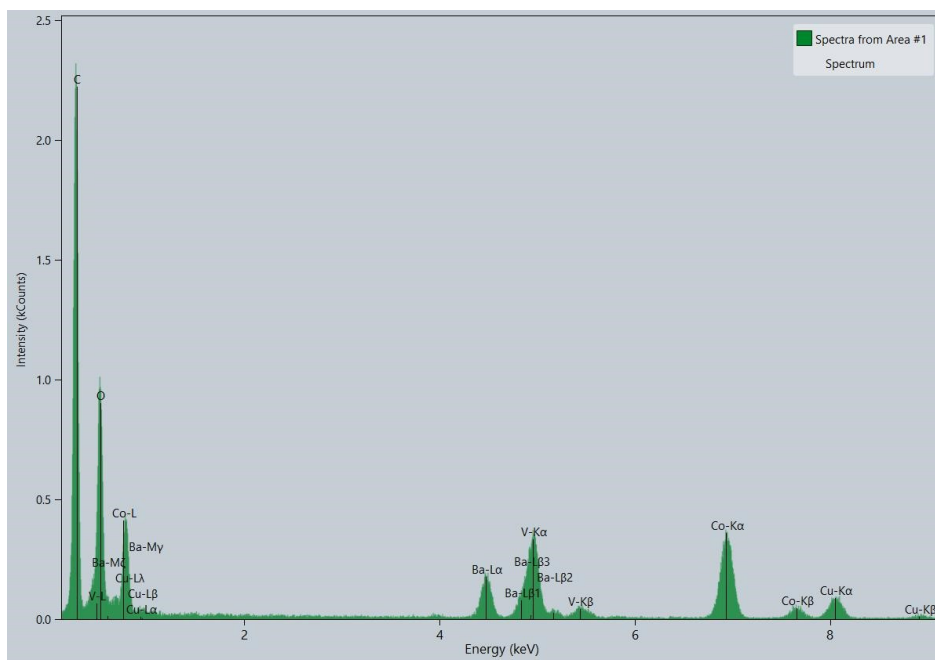


Figure S4. EDS spectrum acquired on several $\text{BaCo}_3(\text{VO}_4)_2(\text{OH})_2$ NPs.

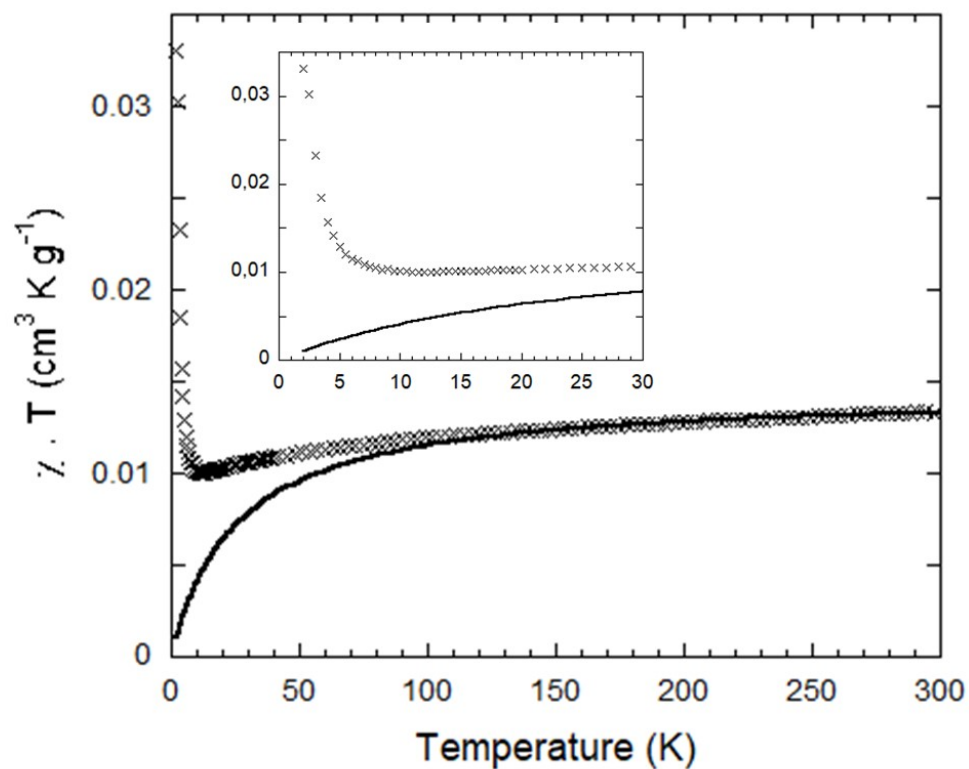


Figure S5. Temperature dependence of the $\chi(T) \cdot T$ product for $\text{BaCo}_3(\text{VO}_4)_2(\text{OH})_2$ NPs. Susceptibility data $\chi(T)$ were acquired under a magnetic field of 100 Oe. The solid line corresponds to a Curie-Weiss fit to the data in the temperature range of 150-300 K. Insert: enlargement of the data below 30 K.

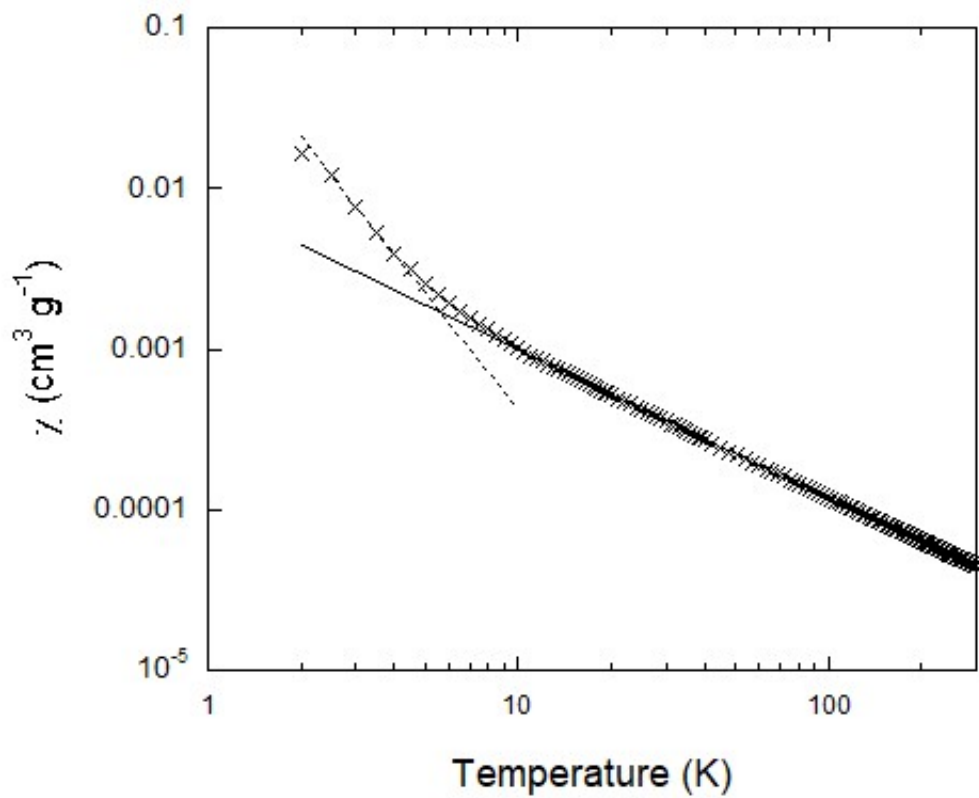


Figure S6. Double-logarithmic plot of the linear susceptibility χ versus temperature T for $\text{BaCo}_3(\text{VO}_4)_2(\text{OH})_2$ NPs. The solid and dashed lines represent power law fits $\chi \propto T^{-\alpha}$ in the temperature ranges of 10-300 K ($\alpha = 0.93$) and of 2.5-5 K ($\alpha = 2.43$), respectively.

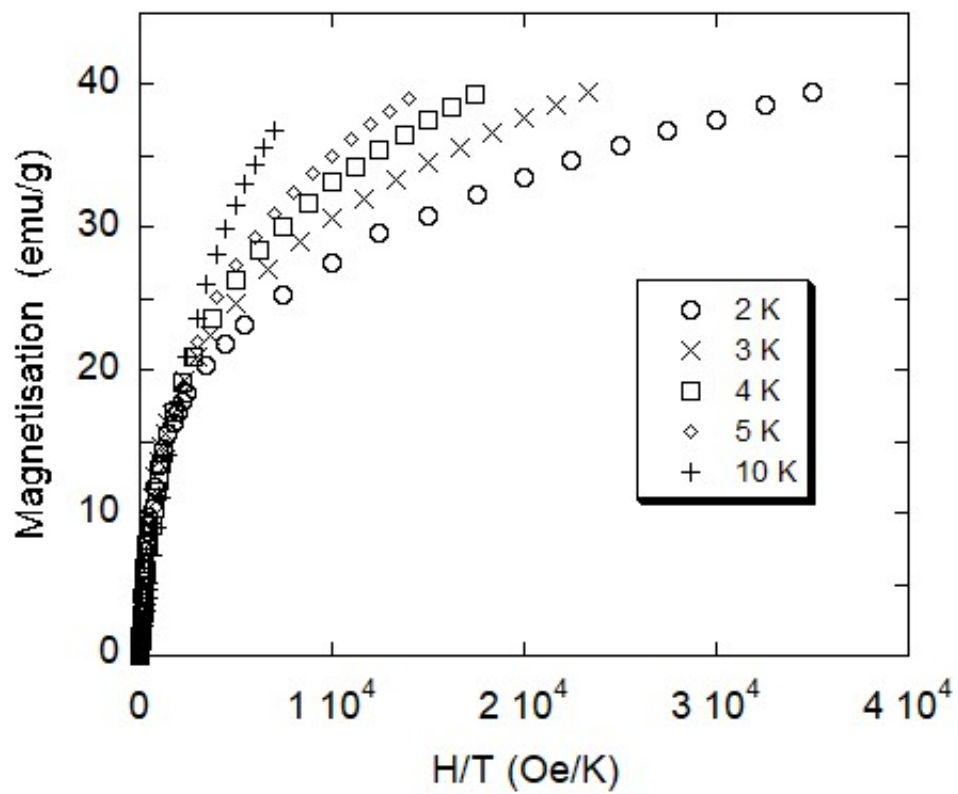


Figure S7. Isothermal magnetization M versus H/T for $\text{BaCo}_3(\text{VO}_4)_2(\text{OH})_2$ NPs at several temperatures below 10 K as indicated.

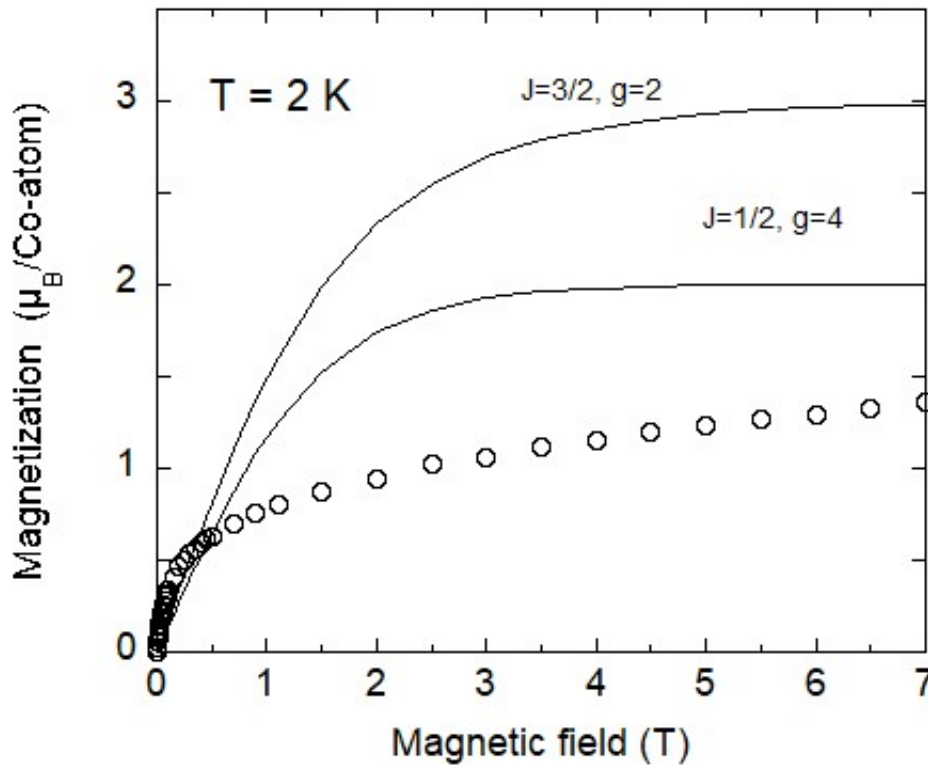


Figure S8. Isothermal magnetization M versus T for $\text{BaCo}_3(\text{VO}_4)_2(\text{OH})_2$ NPs at 2 K. Solid lines depict Brillouin equations for noninteracting magnetic moments, $M = g J \mu_B B_J(g, H, T)$, using J and g values as indicated.

References

- 1 V. Petříček, M. Dušek and L. Palatinus, *Z. Für Krist. - Cryst. Mater.*, 2014, **229**, 345–352.
- 2 R. W. Cheary and A. Coelho, *J. Appl. Crystallogr.*, 1992, **25**, 109–121.
- 3 R. W. Cheary and A. A. Coelho, *J. Appl. Crystallogr.*, 1998, **31**, 851–861.
- 4 R. W. Cheary and A. A. Coelho, *J. Appl. Crystallogr.*, 1998, **31**, 862–868.
- 5 T. Djorđević and L. Karanović, *Acta Crystallogr. C*, 2013, **69**, 114–118.
- 6 P. Stadelmann, JEMS JAVA electron microscopy software., <http://cimewww.epfl.ch/people/stadelmann/jemsWebSite/jems.html>.
- 7 J. Barthel, *Ultramicroscopy*, 2018, **193**, 1–11.